PHOTONICS Research

N-polar InGaN/GaN nanowires: overcoming the efficiency cliff of red-emitting micro-LEDs

A. Pandey,[1] Y. Malhotra,[1] P. Wang,[1] K. Sun,[2] X. Liu,[1] and Z. Mi[1,*]

[1]Department of Electrical Engineering and Computer Science, University of Michigan, Ann Arbor, Michigan 48109, USA
[2]Department of Materials Science and Engineering, University of Michigan, Ann Arbor, Michigan 48109, USA
*Corresponding author: ztmi@umich.edu

Received 9 December 2021; revised 26 January 2022; accepted 23 February 2022; posted 25 February 2022 (Doc. ID 450465); published 29 March 2022

A high efficiency, high brightness, and robust micro or sub-microscale red light emitting diode (LED) is an essential, yet missing, component of the emerging virtual reality and future ultrahigh resolution mobile displays. We report, for the first time, to our knowledge, the demonstration of an N-polar InGaN/GaN nanowire sub-microscale LED emitting in the red spectrum that can overcome the efficiency cliff of conventional red-emitting micro-LEDs. We show that the emission wavelengths of N-polar InGaN/GaN nanowires can be progressively shifted from yellow to orange and red, which is difficult to achieve for conventional InGaN quantum wells or Ga-polar nanowires. Significantly, the optical emission intensity can be enhanced by more than one order of magnitude by employing an *in situ* annealing process of the InGaN active region, suggesting significantly reduced defect formation. LEDs with lateral dimensions as small as ∼0.75 μm, consisting of approximately five nanowires, were fabricated and characterized, which are the smallest red-emitting LEDs ever reported, to our knowledge. A maximum external quantum efficiency ∼1.2% was measured, which is comparable to previously reported conventional quantum well micro-LEDs operating in this wavelength range, while our device sizes are nearly three to five orders of magnitude smaller in surface area.

https://doi.org/10.1364/PRJ.450465

1. INTRODUCTION

Sub-micrometer and nanoscale optoelectronic devices, including light emitting diodes (LEDs) and laser diodes, have drawn considerable attention, as they are essential for future large scale, or ultra-large scale integration of electronic and optoelectronic devices on a single chip. To date, however, it has remained extremely challenging to achieve high efficiency micro or nanoscale optoelectronic devices. One noticeable example is the efficiency cliff related to micro-LEDs, i.e., a drastic reduction in device efficiency with reducing dimensions. Micro-LEDs have been considered as the essential building block for emerging virtual/augmented reality devices and systems, due to their ultrahigh brightness, low power consumption, ultrahigh integration density, superior stability, and long lifetime. Shown in Fig. 1, external quantum efficiency (EQE) in the range of 50%–70% has been commonly measured for AlGaInP-based large area LEDs (lateral dimensions >100 μm), whereas the efficiency drops to negligible values for devices with lateral dimensions of the order of 10 μm.

It is known that AlGaInP-based materials have poor charge carrier confinement, relatively long carrier diffusion length, and large surface recombination [1,2]. In this regard, Ga(In)N-based heterostructures offer stronger carrier confinement, smaller carrier diffusion lengths, as well as a lower level of surface recombination velocity [3]. However, the large lattice mismatch between InN and GaN (∼10%) has prevented the realization of high quality InGaN quantum well heterostructures emitting in the deep visible, i.e., yellow, orange, and red spectra. As such, the efficiency of conventional InGaN quantum well LEDs decreases drastically with increasing wavelengths. Moreover, the efficiency cliff, caused by etch-induced surface damaging with reduced device size, is even more severe than that of AlInGaP-based red LEDs [4–9]. Shown in Fig. 1 are some reported EQE values for InGaN [10–23] and AlGaInP [24–32] based red LEDs with different lateral dimensions. Here, we refer to "red" LEDs as having the dominant emission peak >620 nm [33]. As can be seen from the figure, an EQE of close to ∼20% has been reported for broad area InGaN orange and red LEDs (lateral dimension ∼1000 μm) [10]; however, this falls to only a few percent or less for devices having lateral sizes in the tens of micrometers [18–22]. There exist few reports for red micro-LEDs with lateral device sizes below 10 μm, and the devices presented therein have a maximum EQE of <0.3% [15,16].

In this context, bottom-up InGaN-based nanostructures, e.g., nanowires and nanorods, offer an alternative approach

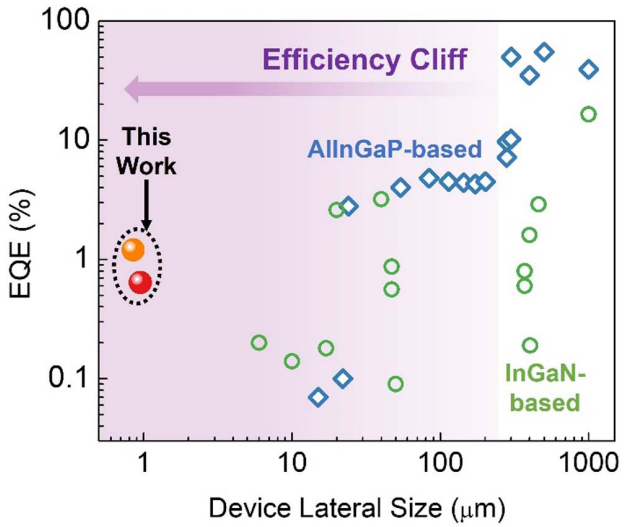

Fig. 1. Variations of peak external quantum efficiency (EQE) of some previously reported red-emitting LEDs (defined as having emission peak >620 nm), showing the presence of the efficiency cliff, i.e., significantly reduced efficiency with decreasing device size. Blue squares: AlInGaP-based red LEDs. Green circles: InGaN-based red LEDs. The results from this work are indicated by the orange and red spheres.

to overcome the efficiency cliff of micro- or nano-LEDs in the deep visible. The bottom-up approach has a major advantage over a top-down etching approach due to the reduced density of surface defects at the edge of the device mesa, commonly associated with plasma-based etching of nitrides [34–36]. (In)GaN nanostructures have been extensively studied previously, showing defect-free structures and enhanced indium incorporation because of their efficient strain relaxation [37–40]. Such InGaN-based nanostructures have shown bright luminescence over a wide spectral range due to their high internal quantum efficiency and light extraction efficiency [41–43]. Further, selective area epitaxy using a patterned mask has also been demonstrated, enabling precise control of the dimensions of nanostructures [44–46]. It has also been shown that through varying the size and spacing of nanostructures, the incorporation of In can be tuned in a single growth step, potentially enabling the monolithic growth of multi-color devices [47–50]. Previous studies on nanostructure LEDs, however, have been largely focused on InGaN-based nanowire devices with mixed or Ga polarity [51–59]. The device performance suffers severely from charge carrier (electron) overflow/leakage and nonradiative parasitic recombination outside of the device active region, leading to very low efficiency [52,60]. Moreover, the pyramid-like morphology associated with Ga-polar nanowires makes it difficult for the fabrication of high efficiency LEDs. These critical issues can be potentially addressed by N-polar InGaN-based nanowires, which are characterized by uniformly flat surfaces that are compatible with standard planar fabrication processes [61–63]. Due to the reversed polarization field in N-polar structures, electron leakage/overflow can be greatly suppressed in N-polar InGaN quantum wells/dots, compared to their Ga-polar counterparts [61]. Recent studies further suggested that the lateral surfaces of N-polar GaN nanowires can form a stable oxynitride layer, which can significantly reduce nonradiative surface recombination [64]. N-polar InGaN also exhibits a higher decomposition temperature than its metal-polar counterpart, thereby allowing for the epitaxy of InGaN at higher temperatures to reduce point defect formation and/or undesired impurity incorporation [65,66]. Despite these promises, there have been few studies of N-polar InGaN-based nanowire micro-LEDs.

Herein, we report, for the first time, the design, epitaxy, and performance characteristics of N-polar InGaN/GaN nanowire-based sub-micrometer scale LEDs operating in the deep visible. We have developed a unique strategy to effectively tune the emission wavelengths of N-polar InGaN/GaN nanowires. It is observed that the emission wavelengths can be shifted from yellow to orange and red by varying the material fluxes and growth temperature. It is further observed that the luminescence efficiency can be enhanced by more than one order of magnitude through an *in situ* annealing process of the InGaN active region to reduce defect formation. LEDs with lateral dimensions as small as ~0.75 μm, consisting of approximately five InGaN nanowires, were fabricated and characterized. A maximum EQE of 1.2% was measured for an unpackaged sub-micrometer scale device, which is comparable to conventional InGaN quantum well orange-red micro-LEDs, while being nearly three to five orders of magnitude smaller in surface area.

2. SELECTIVE AREA GROWTH AND CHARACTERIZATION OF N-POLAR NANOWIRES

Schematically shown in Fig. 2(a) is the N-polar GaN/InGaN nanowire micro-LED heterostructure, which consists of Si-doped GaN, InGaN active region, and Mg-doped GaN contact layer. Prior to the epitaxy of the N-polar nanowires, Si-doped N-polar GaN templates, with thicknesses ~0.8 μm, were first grown on a sapphire substrate utilizing a Veeco GENxplor plasma-assisted molecular beam epitaxial (PA-MBE) system [67]. The grown N-polar GaN substrate was then coated with a 10 nm thick Ti layer, which was patterned with electron beam lithography and dry etching to define the nanowire openings for selective area epitaxy. For this work, we designed several different arrays of nanowires on each sample, within which the nanowire dimensions and spacing were kept constant. For the different arrays, the nanowire diameters varied from 85 to 280 nm, with a pitch varying from 220 to 320 nm. The patterned substrate was then loaded into a Veeco Gen 930 PA-MBE system for the subsequent nanowire growth. Before starting the nanowire growth, the Ti mask on the substrate was nitridated at a thermocouple temperature of 400°C in nitrogen plasma for 10 min. The nanowires started with an initial 500 nm thick n-GaN section, grown at a thermocouple temperature ~880°C, with a nitrogen flow of 0.7 sccm (standard cubic centimeters per minute) and a Ga metal flux $\sim 3 \times 10^{-7}$ Torr (1 Torr = 133.32 Pa) beam equivalent pressure (BEP). For the InGaN active region, a high nitrogen flow of 1.4 sccm was used, and the growth temperature was reduced to ~650°C for sample A and ~635°C for sample B. These samples were further fabricated, as will be discussed below. An optimized growth temperature, higher nitrogen flow rate,

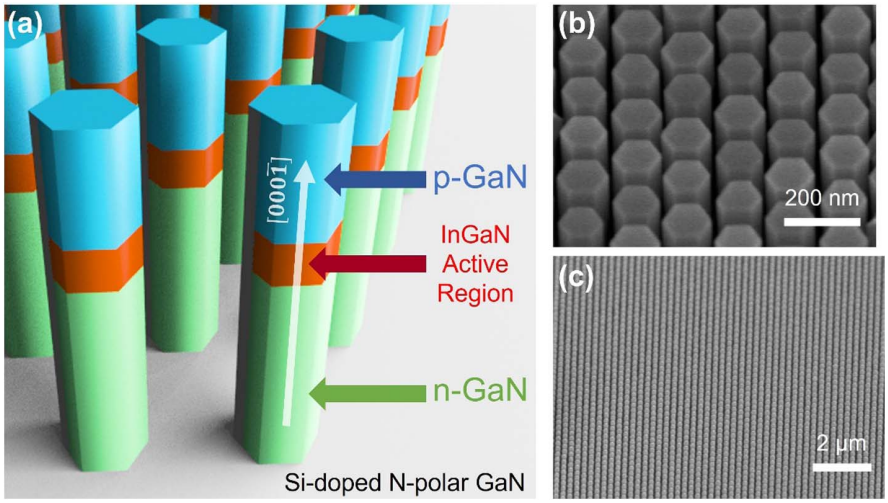

Fig. 2. (a) Schematic illustration of N-polar InGaN/GaN nanowire LED heterostructures grown on N-polar GaN template on sapphire substrate. (b), (c) SEM images of an N-polar InGaN/GaN nanowire array, showing site-controlled epitaxy and high uniformity.

and properly tuned In/Ga flux ratio were found essential to enhance indium incorporation to achieve bright deep visible light emission. The In and Ga BEPs are approximately 1×10^{-7} Torr and 4×10^{-8} Torr, respectively, which can be further varied to tune the emission wavelengths. The thickness of the InGaN active region was kept at 40 and 20 nm for sample A and sample B, respectively. A ∼100 nm thick Mg-doped p-GaN layer was subsequently grown at a thermocouple temperature ∼900°C using a Mg flux of $\sim 3 \times 10^{-8}$ Torr. Shown in Fig. 2(b), the N-polar nanowires display good selectivity and flat *c*-plane morphology. The realization of uniform N-polar InGaN/GaN nanowire arrays is further illustrated in Fig. 2(c).

Attaining efficient long wavelength emission, e.g., orange and red, for InGaN-based LEDs is extremely difficult due to the large lattice mismatch (up to 11%) between InN and GaN, indium phase separation, and quantum-confined Stark effect [68–75]. In this study, to achieve red emission, we performed a detailed investigation of the role of the In/Ga flux ratio, growth temperature for the active region, and the *in situ* annealing of the active region. It was observed that with reducing growth temperature, the emission wavelengths showed a progressive shift toward longer wavelengths. However, the emission intensity showed a significant reduction with reducing growth temperature. Moreover, it remained difficult to achieve spectrally pure red emission (>620 nm). Through detailed growth optimization, it was observed that reduction of Ga flux in the active region could lead to a more significant redshift in emission as opposed to reducing the growth temperature. The redshift with reducing Ga flux can be well explained by the larger bond strength of GaN as compared to InN, which results in the favorable incorporation of Ga in the crystal [76]. Given that the growth of the active region was performed under nitrogen-rich conditions, a significant impact of nitrogen flow on alloy composition was not observed.

The use of a relatively low growth temperature and high nitrogen flow rate in enhancing indium incorporation and achieving red emission also promotes the formation of point defects, e.g., Ga/In vacancies and N-interstitials, which may severely limit the radiative efficiency [42,77,78]. In this regard, to further improve the luminescence efficiency, we developed an *in situ* annealing process for the InGaN active region. This technique has been previously used to reduce the point defect density and improve the emission intensity of InGaN/GaN quantum wells [79,80]. Following the growth of the InGaN segment and a GaN capping layer, a growth interruption was introduced. During the growth interruption, the substrate temperature was raised under a nitrogen soak, and the sample was annealed *in situ* at an elevated temperature of ∼700°C for 3 min. This *in situ* annealing process was found to drastically improve the optical properties. Shown in Fig. 3, with the incorporation of *in situ* annealing, the photoluminescence intensity is enhanced by more than one order of magnitude for nanowires with identical dimensions of ∼200 nm diameter and 240 nm spacing. The photoluminescence involved exciting the sample at room temperature using a 405 nm laser with output power ∼5 mW. The sample emission was collected with an optical fiber and analyzed using a Horiba iHR 550 spectrometer. Detailed studies further suggest that the annealing duration and temperature play an important role. While a higher annealing temperature is more effective in reducing point defect concentration, it can also result in significant blueshift. To minimize indium out-diffusion during the annealing process, the thickness of the GaN capping layer is carefully optimized. The peak emission wavelengths from photoluminescence measurements of the optimized structures sample A and sample B were 620 and 635 nm, respectively.

A cross-sectional specimen for scanning transmission electron microscopy (STEM) study was made from a nanowire LED sample using an *in situ* focused ion beam (FIB) lift-out method performed in a Thermo-Fisher Helios G4 Xe plasma FIB/SEM system at the Michigan Center for Materials Characterization (MCMC). A JEOL-JEM3100R05 TEM system, equipped with double-aberration correctors, was used for imaging the microstructures of the specimen at high spatial

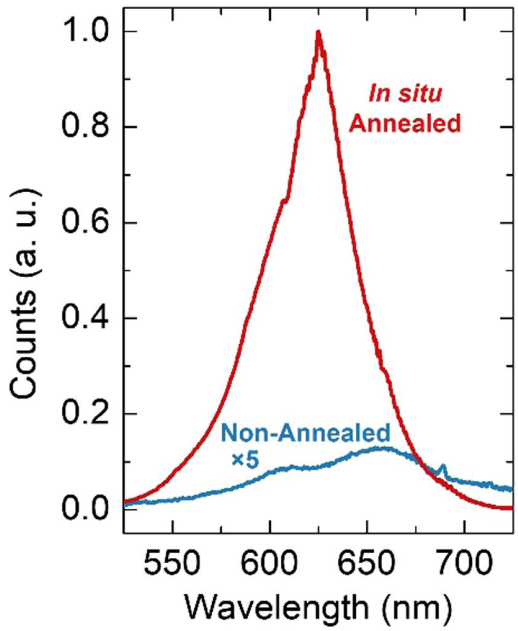

Fig. 3. Photoluminescence spectra of InGaN/GaN nanowire heterostructures measured at room temperature for samples with (red) and without (blue) *in situ* annealing. The intensity of the non-annealed sample has been enhanced by a factor of five.

resolution. The microscope was operated at 300 keV in STEM mode with lens settings that define a probe smaller than 0.1 nm. High-angle annular dark-field (HAADF) imaging was performed together with bright-field (BF) imaging simultaneously. A Thermo-Fisher Talos F200 STEM/TEM system with four silicon drift detectors (SDDs) attached was used for STEM spectrum imaging (SI) using X-ray signals.

Figure 4(a) is a low magnification STEM-HAADF image showing the cross section of a few nanowires. No extended crystal defects could be observed in the images of the nanowires [81]. The InGaN active region (shown as the region with a lighter contrast in the middle of the nanowire) grows axially along the *c*-plane of the nanowire, which contrasts with the growth along the semi-polar planes observed in Ga-polar nanowires [82–84]. While little lateral growth is observed in the nanowires until the start of the active region, following it, there is a noticeable change in nanowire diameter, which is related to the strain relaxation and relatively low growth temperature for this section [39]. The images of the nanowire arrays also show the presence of voids formed in between the nanowires, which are a result of the deposition of insulating layers to electrically isolate the nanowires. A magnified STEM-HAADF image of the InGaN active region within the nanowire in the center of Fig. 4(a) is shown in Fig. 4(b) and its atom-resolved HAADF image in Fig. 4(c). A relatively inhomogeneous InGaN segment is observed, which could be a direct consequence of the composition-pulling effect previously observed in high In composition InGaN layers [40,85,86]. In addition, the *in situ* thermal annealing process may contribute to the interface diffusion of indium atoms [87–89]. Figure 4(d) shows Ga and In distributions inside part of the nanowire including the InGaN active region. The In and Ga elemental distributions along the outlined dotted band shown in Fig. 4(d) are quantified in Fig. 4(e), confirming the formation of the In-rich InGaN active region.

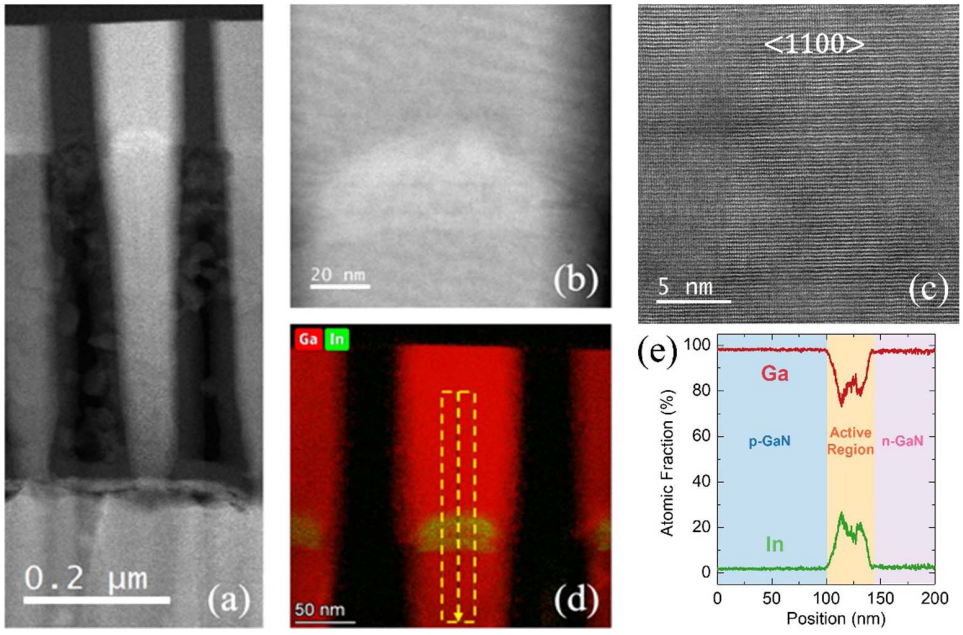

Fig. 4. (a) Cross-sectional STEM-HAADF image of nanowires. (b) Magnified STEM-HAADF image of the InGaN active region in the nanowire shown in the middle of (a). (c) Atomic-scale HAADF image of the InGaN active region. (d) Color mixed element map collected from a part of the nanowire with the InGaN active region included by STEM-SI using X-ray signals showing the distributions of Ga (red) and In (green). (e) Ga and In elemental profiles along the dotted band outlined in (d), with the different sections of the nanowire shown as shaded regions.

3. FABRICATION OF MICRO-LEDS AND DEVICE MEASUREMENTS

N-polar InGaN/GaN nanowire micro-LEDs were then fabricated. First the nanowire arrays were passivated with an insulating Al_2O_3 layer deposited by atomic layer deposition. An etch-back step using reactive ion etching (RIE) was performed to expose the top p-GaN contact layer of the nanowires. The sample was coated with a 300 nm thick SiO_2 layer using plasma-enhanced chemical vapor deposition. Lithography was used to define sub-micrometer current-injection vias and n-contact windows, followed by the removal of the SiO_2 layer using RIE. The sub-micrometer openings varied in lateral dimensions of 750 nm to 1 μm, and a schematic of the current-injection window is shown in Fig. 5(a). Shown in Fig. 5(b) is an SEM image of a sub-micrometer scale device injection opening, consisting of five nanowires, which is the smallest red LED device, to our knowledge. The via opened in the insulation layer is indicated by the dashed line in the figure. The n-metal contact consisting of Ti (20 nm)/Au (100 nm) was deposited on the Si-doped N-polar GaN template. The p-type contact to the top of the nanowires consisted of a Ni (5 nm)/Au (5 nm)/indium tin oxide (180 nm) stack. The contacts were annealed at 550°C for 1 min in an ambient of forming gas. The fabricated micro-LEDs were designed to emit light from the back of the substrate (through the sapphire). To maximize light extraction, the device contacts were covered with a reflective electrode comprising Ag (50 nm)/Al (100 nm)/Ni (20 nm)/Au (50 nm). Subsequently, the micro-LEDs were characterized directly on-wafer without any packaging.

Shown in Fig. 5(c), depending on the growth conditions and nanowire sizes, electroluminescence (EL) emission in the wavelength range of ~550 to 650 nm was measured. We observed a progressive redshift for the emission from devices with increasing diameter of the nanowires, while keeping the same nanowire pitch. This phenomenon has been previously observed in MBE-grown InGaN/GaN nanowire arrays, and it has been attributed to the shadowing of incident metal atom beams by neighboring nanowire columns [47–49]. Further, the lower growth temperature of sample B enables more redshifted emission from a nanowire array with identical dimensions to that on sample A. Devices A and B from samples A and B, respectively, were further studied. Devices A and B had lateral sizes of ~800 and 950 nm, respectively. The designed nanowire diameter and pitch for the array containing device A was 140 and 220 nm, respectively, while device B was fabricated in an array having a nanowire diameter of 195 nm and a pitch of 240 nm. Shown in Fig. 5(d), the devices exhibit similar *J-V* characteristics, reaching a current density

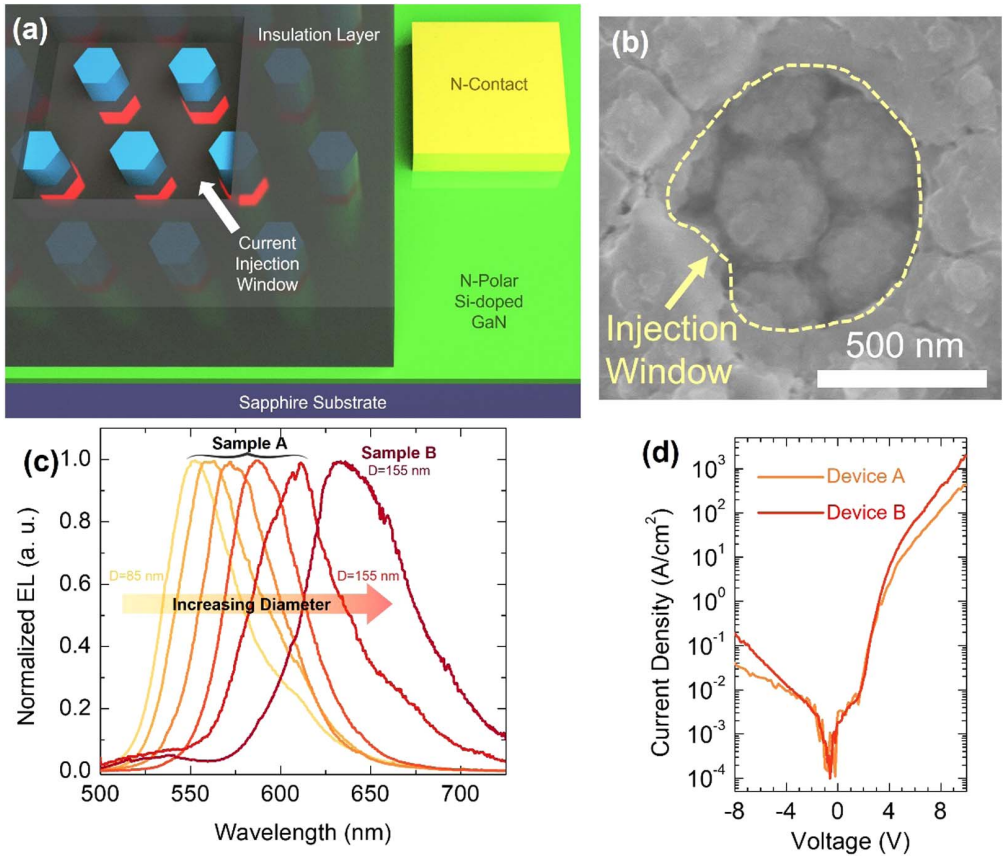

Fig. 5. (a) Schematic of the InGaN/GaN micro-LED device, showing current injection window before depositing p-metal contact. (b) SEM image of the submicrometer-scale device via, with the injection window indicated by the yellow dashed curve. (c) EL spectra measured for different devices, showing the tunability of the emission wavelength across the yellow-red wavelength range of the visible spectrum. For the devices shown, the sample names and the designed nanowire diameters are specified, while the nanowire pitch is kept fixed at 280 nm. (d) *J-V* characteristics for devices A and B, shown as orange and red curves, respectively.

of ~10 A/cm^2 at a voltage of ~4 V. The reverse bias current is extremely low, suggesting the formation of a well-defined p-n junction. The turn-on voltage for the devices can be further improved through optimization of the p-type contact and device fabrication process.

EL spectra of the devices were thereafter measured at room temperature. Figure 6(a) shows the EL spectra for device A at injection currents from 0.5 to 6 A/cm^2, with the main peak located at ~620 nm. The emission spectra of device B (peak emission ~635 nm) are shown in Fig. 6(b). The relatively broad emission is due to the compositional non-uniformity in the active region, which has been commonly seen for In-rich InGaN structures. Figures 6(c) and 6(d) plot the variation of the full-width at half-maximum (FWHM) and peak position, respectively, for devices A and B. The initial decrease in the measured FWHM may be related to the redistribution of carriers between localized states within the inhomogeneous InGaN segment [23,90,91]. The devices also exhibit a blueshift with increasing injection, with the emission peak varying by up to ~20 nm for the grown samples. Such a wavelength shift has been attributed to the screening of the strong polarization fields present in the InGaN layer of the device [74,92]. The measured wavelength shift with increasing injection is comparable to or less than that of previously reported red InGaN LEDs [15,16,18,22]. The large FWHM and shift in EL peak make it challenging to attain bright red emission with InGaN LEDs, which is crucial for display applications [93]. To realize efficient and stable red emission over a wide range of output power levels, such bottom-up nanostructures can be incorporated into a properly designed photonic crystal, which can result in much narrower and stable linewidths [82,94,95].

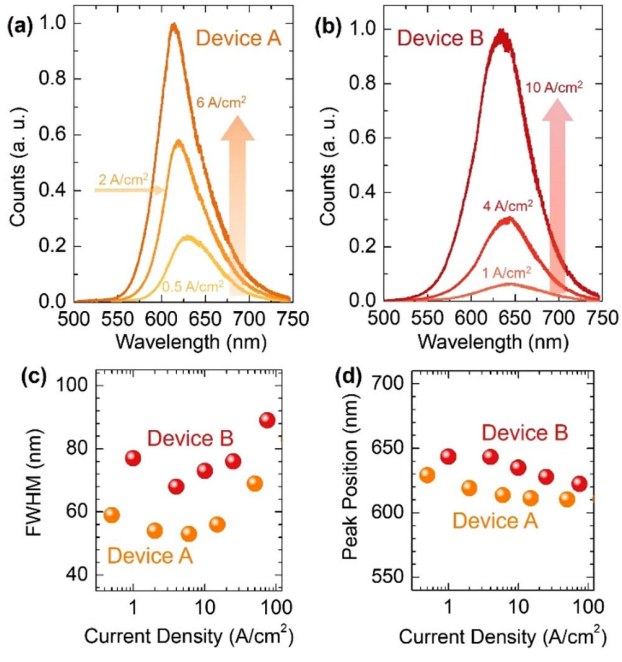

Fig. 6. (a) EL spectra measured for device A from an injection current of 0.5–6 A/cm^2. (b) EL spectra measured for device B from an injection current of 1–10 A/cm^2. Variation of the (c) FWHM and (d) peak position, measured from the EL spectra for devices at different injection currents.

For measuring the output power from the fabricated devices, we used a Keithley 2400 SMU to bias the device in continuous-wave (CW) mode, while measuring the device output power on-wafer, using a calibrated Newport 818-ST2-UV/DB detector, through the backside of the sapphire substrate. The measured EQE at different injection currents is plotted for device A, shown in Fig. 7. The EQE shows a peak at relatively low current densities of ~0.5 A/cm^2. For comparison, previously reported InGaN-based red-emitting quantum well LEDs exhibit efficiency peak at relatively low current densities below 20 A/cm^2 [10,18,23]. It is generally observed that the peak efficiency occurs at a lower current density level for LED heterostructures with a lower level of Shockley–Read–Hall (SRH) non-radiative recombination [96,97]. The efficient surface strain relaxation and the use of *in situ* annealing would reduce point defect formation within the active region of the nanowires [40,79] we have studied, which could reduce SRH recombination, improving the device efficiency. As the devices were measured on-wafer, suitable packaging should greatly increase the light extraction efficiency. The selective area growth of bottom-up nanowires can be further exploited to form photonic crystals, which have previously been used to increase the light extraction efficiency, generate highly directional sources of light, and also form guiding modes that can be used to narrow the linewidths of LEDs, or to realize surface emitting lasers [82,94,98,99]—all of which are future possibilities that are compatible with the growth of the N-polar devices discussed in this work. The sidewall of N-polar GaN nanowires has been shown to be characterized by the presence of N-rich clusters, which can further help minimize surface oxidation and impurity incorporation, thereby reducing nonradiative surface recombination [64,100]. Efficiency droop, however, is measured with increasing injection current. Efficiency droop has

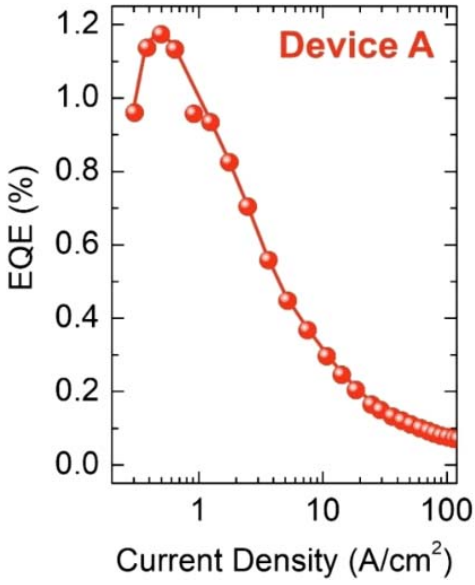

Fig. 7. Variation of EQE with current density for device A. Due to the very low power under low injection conditions, the error bar is estimated to be 15% for the derived EQE in the low current density regime.

been commonly measured in GaN-based LEDs, with the underlying causes including Auger recombination, electron overflow, and carrier delocalization [101–105]. For nanowire devices, carrier overflow/leakage tends to be more severe due to the strong influence of nonradiative surface recombination, which is exacerbated by the large nanowire surface area. These effects have been shown to cause a sharp droop in the efficiency of N-polar green-emitting micro-LEDs at low injection currents, limiting their high-power operation [106]. Recent studies of tunnel-junction-based blue LEDs suggested efficiency droop can be significantly reduced by enhancing charge carrier (hole) injection into the device active region, suggesting electron overflow is the primary cause for the observed efficiency droop [61,107]. In this regard, the carrier leakage, electron overflow, and efficiency droop can be reduced by incorporating a core–shell heterostructure surrounding the device active region and a suitable electron blocking layer in future developments.

4. SUMMARY

In summary, we have developed red-emitting N-polar InGaN/GaN nanowire heterostructures and have further demonstrated the smallest size red-emitting LEDs ever reported, to the best of our knowledge. The device surface area is nearly three orders of magnitude smaller than some of the previously reported InGaN quantum well red micro-LEDs. An EQE ~1.2% was measured directly on-wafer for a sub-micrometer scale device, which is comparable to or better than that of conventional red InGaN quantum-well-based micro-LEDs. Detailed studies further suggest that the performance is largely limited by severe efficiency droop, due to electron overflow, which can be addressed by improving the device design and epitaxy process. This work provides a path to overcome the efficiency cliff of deep visible micro-LEDs, which are relevant for a broad range of applications including mobile displays and virtual/augmented reality devices and systems.

Funding. University of Michigan; National Science Foundation (#DMR-0723032).

Acknowledgment. Part of the TEM studies in this work were technically supported by the Michigan Center for Materials Characterization.

Disclosures. Some intellectual property related to GaN-based nanowires was licensed to NS Nanotech Inc., which was co-founded by Z. Mi. The University of Michigan and Mi have a financial interest in NS Nanotech, Inc.

Data Availability. Data underlying the results presented in this paper are not publicly available at this time but may be obtained from the authors upon reasonable request.

REFERENCES

1. J.-I. Shim, D.-P. Han, H. Kim, D.-S. Shin, G.-B. Lin, D. S. Meyaard, Q. Shan, J. Cho, E. Fred Schubert, and H. Shim, "Efficiency droop in AlGaInP and GaInN light-emitting diodes," Appl. Phys. Lett. **100**, 111106 (2012).
2. M. S. Wong, J. A. Kearns, C. Lee, J. M. Smith, C. Lynsky, G. Lheureux, H. Choi, J. Kim, C. Kim, and S. Nakamura, "Improved performance of AlGaInP red micro-light-emitting diodes with sidewall treatments," Opt. Express **28**, 5787–5793 (2020).
3. M. Boroditsky, I. Gontijo, M. Jackson, R. Vrijen, E. Yablonovitch, T. Krauss, C.-C. Cheng, A. Scherer, R. Bhat, and M. Krames, "Surface recombination measurements on III-V candidate materials for nanostructure light-emitting diodes," J. Appl. Phys. **87**, 3497–3504 (2000).
4. F. Olivier, S. Tirano, L. Dupré, B. Aventurier, C. Largeron, and F. Templier, "Influence of size-reduction on the performances of GaN-based micro-LEDs for display application," J. Lumin. **191**, 112–116 (2017).
5. M. S. Wong, D. Hwang, A. I. Alhassan, C. Lee, R. Ley, S. Nakamura, and S. P. DenBaars, "High efficiency of III-nitride micro-light-emitting diodes by sidewall passivation using atomic layer deposition," Opt. Express **26**, 21324–21331 (2018).
6. D. Hwang, A. Mughal, C. D. Pynn, S. Nakamura, and S. P. DenBaars, "Sustained high external quantum efficiency in ultrasmall blue III–nitride micro-LEDs," Appl. Phys. Express **10**, 032101 (2017).
7. F. Olivier, A. Daami, C. Licitra, and F. Templier, "Shockley-Read-Hall and Auger non-radiative recombination in GaN based LEDs: a size effect study," Appl. Phys. Lett. **111**, 022104 (2017).
8. K. A. Bulashevich and S. Y. Karpov, "Impact of surface recombination on efficiency of III-nitride light-emitting diodes," Phys. Status Solidi RRL **10**, 480–484 (2016).
9. E. F. Schubert, *Light-Emitting Diodes* (Cambridge University, 2006).
10. S. Zhang, J. Zhang, J. Gao, X. Wang, C. Zheng, M. Zhang, X. Wu, L. Xu, J. Ding, and Z. Quan, "Efficient emission of InGaN-based light-emitting diodes: toward orange and red," Photon. Res. **8**, 1671–1675 (2020).
11. J.-I. Hwang, R. Hashimoto, S. Saito, and S. Nunoue, "Development of InGaN-based red LED grown on (0001) polar surface," Appl. Phys. Express **7**, 071003 (2014).
12. D. Iida, K. Niwa, S. Kamiyama, and K. Ohkawa, "Demonstration of InGaN-based orange LEDs with hybrid multiple-quantum-wells structure," Appl. Phys. Express **9**, 111003 (2016).
13. D. Iida, Z. Zhuang, P. Kirilenko, M. Velazquez-Rizo, M. A. Najmi, and K. Ohkawa, "633-nm InGaN-based red LEDs grown on thick underlying GaN layers with reduced in-plane residual stress," Appl. Phys. Lett. **116**, 162101 (2020).
14. D. Iida, Z. Zhuang, P. Kirilenko, M. Velazquez-Rizo, and K. Ohkawa, "Demonstration of low forward voltage InGaN-based red LEDs," Appl. Phys. Express **13**, 031001 (2020).
15. S. S. Pasayat, C. Gupta, M. S. Wong, R. Ley, M. J. Gordon, S. P. DenBaars, S. Nakamura, S. Keller, and U. K. Mishra, "Demonstration of ultra-small (<10 μm) 632 nm red InGaN micro-LEDs with useful on-wafer external quantum efficiency (>0.2%) for mini-displays," Appl. Phys. Express **14**, 011004 (2021).
16. A. Dussaigne, P. L. Maitre, H. Haas, J.-C. Pillet, F. Barbier, A. Grenier, N. Michit, A. Jannaud, R. Templier, D. Vaufrey, F. Rol, O. Ledoux, and D. Sotta, "Full InGaN red (625 nm) micro-LED (10 μm) demonstration on a relaxed pseudo-substrate," Appl. Phys. Express **14**, 092011 (2021).
17. D. Iida, S. Lu, S. Hirahara, K. Niwa, S. Kamiyama, and K. Ohkawa, "Enhanced light output power of InGaN-based amber LEDs by strain-compensating AlN/AlGaN barriers," J. Cryst. Growth **448**, 105–108 (2016).
18. A. Dussaigne, F. Barbier, B. Damilano, S. Chenot, A. Grenier, A. Papon, B. Samuel, B. Ben Bakir, D. Vaufrey, J. Pillet, A. Gasse, O. Ledoux, M. Rozhavskaya, and D. Sotta, "Full InGaN red light emitting diodes," J. Appl. Phys. **128**, 135704 (2020).
19. Z. Zhuang, D. Iida, and K. Ohkawa, "Investigation of InGaN-based red/green micro-light-emitting diodes," Opt. Lett. **46**, 1912–1915 (2021).
20. P. Li, A. David, H. Li, H. Zhang, C. Lynsky, Y. Yang, M. Iza, J. S. Speck, S. Nakamura, and S. P. DenBaars, "High-temperature electroluminescence properties of InGaN red 40 × 40 μm^2 micro-light-emitting diodes with a peak external quantum efficiency of 3.2%," Appl. Phys. Lett. **119**, 231101 (2021).

21. Z. Zhuang, D. Iida, M. Velazquez-Rizo, and K. Ohkawa, "630-nm red InGaN micro-light-emitting diodes (<20 μm × 20 μm) exceeding 1 mW/mm^2 for full-color micro-displays," Photon. Res. **9**, 1796–1802 (2021).
22. P. Li, H. Li, H. Zhang, C. Lynsky, M. Iza, J. S. Speck, S. Nakamura, and S. P. DenBaars, "Size-independent peak external quantum efficiency (>2%) of InGaN red micro-light-emitting diodes with an emission wavelength over 600 nm," Appl. Phys. Lett. **119**, 081102 (2021).
23. Z. Zhuang, D. Iida, P. Kirilenko, and K. Ohkawa, "Improved performance of InGaN-based red light-emitting diodes by micro-hole arrays," Opt. Express **29**, 29780–29788 (2021).
24. K. Streubel, U. Helin, V. Oskarsson, E. Bäcklin, and Å. Johansson, "High brightness visible (660 nm) resonant-cavity light-emitting diode," IEEE Photon. Technol. Lett. **10**, 1685–1687 (1998).
25. C. Y. Lee, J. Y. Su, and C. M. Kuo, "630-nm n-type modulation-doped AlGaInP-AlInP multiquantum-well light-emitting diode," IEEE Photon. Technol. Lett. **18**, 25–27 (2006).
26. R. Windisch, R. Butendeich, S. Illek, S. Kugler, R. Wirth, H. Zull, and K. Streubel, "100-lm/W InGaAlP thin-film light-emitting diodes with buried microreflectors," IEEE Photon. Technol. Lett. **19**, 774–776 (2007).
27. C. Rooman, S. D. Jonge, C. Karnutsch, K. Streubel, M. Kuijk, B. Dutta, G. Borghs, and P. L. Heremans, "Wafer-bonded thin-film surface-roughened light-emitting diodes," Proc. SPIE **4996**, 40–45 (2003).
28. M. R. Krames, M. Ochiai-Holcomb, G. Höfler, C. Carter-Coman, E. Chen, I.-H. Tan, P. Grillot, N. Gardner, H. Chui, and J.-W. Huang, "High-power truncated-inverted-pyramid $(Al_xGa_{1-x})_{0.5}In_{0.5}P$/GaP light-emitting diodes exhibiting >50% external quantum efficiency," Appl. Phys. Lett. **75**, 2365–2367 (1999).
29. X.-L. Wang, N. Kumagai, and G.-D. Hao, "High-efficiency, high-power AlGaInP thin-film LEDs with micron-sized truncated cones as light-extraction structures," Phys. Status Solidi A **215**, 1700562 (2018).
30. J.-T. Oh, S.-Y. Lee, Y.-T. Moon, J. H. Moon, S. Park, K. Y. Hong, K. Y. Song, C. Oh, J.-I. Shim, and H.-H. Jeong, "Light output performance of red AlGaInP-based light emitting diodes with different chip geometries and structures," Opt. Express **26**, 11194–11200 (2018).
31. C. H. Yen, Y. J. Liu, K. H. Yu, P. L. Lin, T. P. Chen, L. Y. Chen, T. H. Tsai, N. Y. Huang, C. Y. Lee, and W. C. Liu, "On an AlGaInP-based light-emitting diode with an ITO direct ohmic contact structure," IEEE Electron Device Lett. **30**, 359–361 (2009).
32. R. Wirth, C. Karnutsch, S. Kugler, and K. Streubel, "High-efficiency resonant-cavity LEDs emitting at 650 nm," IEEE Photon. Technol. Lett. **13**, 421–423 (2001).
33. D. Malacara, *Color Vision and Colorimetry: Theory and Applications* (SPIE, 2011).
34. R. Qiu, H. Lu, D. Chen, R. Zhang, and Y. Zheng, "Optimization of inductively coupled plasma deep etching of GaN and etching damage analysis," Appl. Surf. Sci. **257**, 2700–2706 (2011).
35. J. Ladroue, A. Meritan, M. Boufnichel, P. Lefaucheux, P. Ranson, and R. Dussart, "Deep GaN etching by inductively coupled plasma and induced surface defects," J. Vac. Sci. Technol. A **28**, 1226–1233 (2010).
36. M. Hartensveld, G. Ouin, C. Liu, and J. Zhang, "Effect of KOH passivation for top-down fabricated InGaN nanowire light emitting diodes," J. Appl. Phys. **126**, 183102 (2019).
37. E. Ertekin, P. A. Greaney, D. Chrzan, and T. D. Sands, "Equilibrium limits of coherency in strained nanowire heterostructures," J. Appl. Phys. **97**, 114325 (2005).
38. F. Glas, "Critical dimensions for the plastic relaxation of strained axial heterostructures in free-standing nanowires," Phys. Rev. B **74**, 121302 (2006).
39. G. Tourbot, C. Bougerol, F. Glas, L. F. Zagonel, Z. Mahfoud, S. Meuret, P. Gilet, M. Kociak, B. Gayral, and B. Daudin, "Growth mechanism and properties of InGaN insertions in GaN nanowires," Nanotechnology **23**, 135703 (2012).
40. G. Tourbot, C. Bougerol, A. Grenier, M. Den Hertog, D. Sam-Giao, D. Cooper, P. Gilet, B. Gayral, and B. Daudin, "Structural and optical properties of InGaN/GaN nanowire heterostructures grown by PA-MBE," Nanotechnology **22**, 075601 (2011).
41. K. Kishino, A. Kikuchi, H. Sekiguchi, and S. Ishizawa, "InGaN/GaN nanocolumn LEDs emitting from blue to red," Proc. SPIE **6473**, 64730T (2007).
42. X. Zhang, H. Lourenço-Martins, S. Meuret, M. Kociak, B. Haas, J.-L. Rouvière, P.-H. Jouneau, C. Bougerol, T. Auzelle, and D. Jalabert, "InGaN nanowires with high InN molar fraction: growth, structural and optical properties," Nanotechnology **27**, 195704 (2016).
43. S. Deshpande, T. Frost, L. Yan, S. Jahangir, A. Hazari, X. Liu, J. Mirecki-Millunchick, Z. Mi, and P. Bhattacharya, "Formation and nature of InGaN quantum dots in GaN nanowires," Nano Lett. **15**, 1647–1653 (2015).
44. H. Sekiguchi, K. Kishino, and A. Kikuchi, "Ti-mask selective-area growth of GaN by RF-plasma-assisted molecular-beam epitaxy for fabricating regularly arranged InGaN/GaN nanocolumns," Appl. Phys. Express **1**, 124002 (2008).
45. K. Kishino, T. Hoshino, S. Ishizawa, and A. Kikuchi, "Selective-area growth of GaN nanocolumns on titanium-mask-patterned silicon (111) substrates by RF-plasma-assisted molecular-beam epitaxy," Electron. Lett. **44**, 819–821 (2008).
46. S. D. Hersee, X. Sun, and X. Wang, "The controlled growth of GaN nanowires," Nano Lett. **6**, 1808–1811 (2006).
47. H. Sekiguchi, K. Kishino, and A. Kikuchi, "Emission color control from blue to red with nanocolumn diameter of InGaN/GaN nanocolumn arrays grown on same substrate," Appl. Phys. Lett. **96**, 231104 (2010).
48. K. Kishino, A. Yanagihara, K. Ikeda, and K. Yamano, "Monolithic integration of four-colour InGaN-based nanocolumn LEDs," Electron. Lett. **51**, 852–854 (2015).
49. K. Kishino, K. Nagashima, and K. Yamano, "Monolithic integration of InGaN-based nanocolumn light-emitting diodes with different emission colors," Appl. Phys. Express **6**, 012101 (2012).
50. Y.-H. Ra, R. Wang, S. Y. Woo, M. Djavid, S. M. Sadaf, J. Lee, G. A. Botton, and Z. Mi, "Full-color single nanowire pixels for projection displays," Nano Lett. **16**, 4608–4615 (2016).
51. H. P. T. Nguyen, K. Cui, S. Zhang, S. Fathololoumi, and Z. Mi, "Full-color InGaN/GaN dot-in-a-wire light emitting diodes on silicon," Nanotechnology **22**, 445202 (2011).
52. H. P. T. Nguyen, M. Djavid, S. Y. Woo, X. Liu, A. T. Connie, S. Sadaf, Q. Wang, G. A. Botton, I. Shih, and Z. Mi, "Engineering the carrier dynamics of InGaN nanowire white light-emitting diodes by distributed p-AlGaN electron blocking layers," Sci. Rep. **5**, 7744 (2015).
53. C. Zhao, N. Alfaraj, R. C. Subedi, J. W. Liang, A. A. Alatawi, A. A. Alhamoud, M. Ebaid, M. S. Alias, T. K. Ng, and B. S. Ooi, "III-nitride nanowires on unconventional substrates: From materials to optoelectronic device applications," Prog. Quantum Electron. **61**, 1–31 (2018).
54. M. Asad, R. Wang, Y.-H. Ra, P. Gavirneni, Z. Mi, and W. S. Wong, "Optically invariant InGaN nanowire light-emitting diodes on flexible substrates under mechanical manipulation," npj Flexible Electron. **3**, 16 (2019).
55. R. Wang, X. Liu, I. Shih, and Z. Mi, "High efficiency, full-color AlInGaN quaternary nanowire light emitting diodes with spontaneous core-shell structures on Si," Appl. Phys. Lett. **106**, 261104 (2015).
56. H. P. T. Nguyen, S. Zhang, A. T. Connie, M. G. Kibria, Q. Wang, I. Shih, and Z. Mi, "Breaking the carrier injection bottleneck of phosphor-free nanowire white light-emitting diodes," Nano Lett. **13**, 5437–5442 (2013).
57. M. Nami, A. Rashidi, M. Monavarian, S. Mishkat-Ul-Masabih, A. K. Rishinaramangalam, S. R. Brueck, and D. Feezell, "Electrically injected GHz-class GaN/InGaN core–shell nanowire-based μLEDs: carrier dynamics and nanoscale homogeneity," ACS Photon. **6**, 1618–1625 (2019).
58. M. Philip, D. Choudhary, M. Djavid, K. Le, J. Piao, and H. Nguyen, "High efficiency green/yellow and red InGaN/AlGaN nanowire light-emitting diodes grown by molecular beam epitaxy," J. Sci.: Adv. Mater. Devices **2**, 150–155 (2017).
59. G. Zhang, Z. Li, X. Yuan, F. Wang, L. Fu, Z. Zhuang, F.-F. Ren, B. Liu, R. Zhang, and H. H. Tan, "Single nanowire green InGaN/GaN light emitting diodes," Nanotechnology **27**, 435205 (2016).

60. H. P. T. Nguyen, K. Cui, S. Zhang, M. Djavid, A. Korinek, G. A. Botton, and Z. Mi, "Controlling electron overflow in phosphor-free InGaN/GaN nanowire white light-emitting diodes," Nano Lett. **12**, 1317–1323 (2012).
61. F. Akyol, D. Nath, S. Krishnamoorthy, P. Park, and S. Rajan, "Suppression of electron overflow and efficiency droop in N-polar GaN green light emitting diodes," Appl. Phys. Lett. **100**, 111118 (2012).
62. Y.-K. Kuo, S.-H. Horng, S.-H. Yen, M.-C. Tsai, and M.-F. Huang, "Effect of polarization state on optical properties of blue-violet InGaN light-emitting diodes," Appl. Phys. A **98**, 509–515 (2010).
63. S.-H. Yen and Y.-K. Kuo, "Polarization-dependent optical characteristics of violet InGaN laser diodes," J. Appl. Phys. **103**, 103115 (2008).
64. G. Zeng, T. A. Pham, S. Vanka, G. Liu, C. Song, J. K. Cooper, Z. Mi, T. Ogitsu, and F. M. Toma, "Development of a photoelectrochemically self-improving Si/GaN photocathode for efficient and durable H 2 production," Nat. Mater. **20**, 1130–1135 (2021).
65. S. Keller, N. Fichtenbaum, M. Furukawa, J. Speck, S. DenBaars, and U. Mishra, "Growth and characterization of N-polar InGaN/GaN multiquantum wells," Appl. Phys. Lett. **90**, 191908 (2007).
66. D. N. Nath, E. Gür, S. A. Ringel, and S. Rajan, "Molecular beam epitaxy of N-polar InGaN," Appl. Phys. Lett. **97**, 071903 (2010).
67. P. Wang, D. Wang, B. Wang, S. Mohanty, S. Diez, Y. Wu, Y. Sun, E. Ahmadi, and Z. Mi, "N-polar ScAlN and HEMTs grown by molecular beam epitaxy," Appl. Phys. Lett. **119**, 082101 (2021).
68. M. H. Crawford, "LEDs for solid-state lighting: performance challenges and recent advances," IEEE J. Sel. Top. Quantum Electron. **15**, 1028–1040 (2009).
69. T. Mukai, M. Yamada, and S. Nakamura, "Characteristics of InGaN-based UV/blue/green/amber/red light-emitting diodes," Jpn. J. Appl. Phys. **38**, 3976 (1999).
70. T. Langer, A. Kruse, F. A. Ketzer, A. Schwiegel, L. Hoffmann, H. Jönen, H. Bremers, U. Rossow, and A. Hangleiter, "Origin of the "green gap": Increasing nonradiative recombination in indium-rich GaInN/GaN quantum well structures," Phys. Status Solidi C **8**, 2170–2172 (2011).
71. M. Rao, D. Kim, and S. Mahajan, "Compositional dependence of phase separation in InGaN layers," Appl. Phys. Lett. **85**, 1961–1963 (2004).
72. B. Pantha, J. Li, J. Lin, and H. Jiang, "Evolution of phase separation in In-rich InGaN alloys," Appl. Phys. Lett. **96**, 232105 (2010).
73. I. H. Ho and G. Stringfellow, "Solid phase immiscibility in GaInN," Appl. Phys. Lett. **69**, 2701–2703 (1996).
74. T. Takeuchi, S. Sota, M. Katsuragawa, M. Komori, H. Takeuchi, H. Amano, and I. Akasaki, "Quantum-confined Stark effect due to piezoelectric fields in GaInN strained quantum wells," Jpn. J. Appl. Phys. **36**, L382 (1997).
75. J. Wu, "When group-III nitrides go infrared: new properties and perspectives," J. Appl. Phys. **106**, 011101 (2009).
76. A. Trampert, O. Brandt, and K. Ploog, "Crystal structure of group III nitrides," in *Semiconductors and Semimetals* (Elsevier, 1997), Vol. **50**, pp. 167–192.
77. D. A. Browne, E. C. Young, J. R. Lang, C. A. Hurni, and J. S. Speck, "Indium and impurity incorporation in InGaN films on polar, nonpolar, and semipolar GaN orientations grown by ammonia molecular beam epitaxy," J. Vac. Sci. Technol. A **30**, 041513 (2012).
78. H. Komaki, T. Nakamura, R. Katayama, K. Onabe, M. Ozeki, and T. Ikari, "Growth of In-rich InGaN films on sapphire via GaN layer by RF-MBE," J. Cryst. Growth **301**, 473–477 (2007).
79. N. A. Kaufmann, A. Dussaigne, D. Martin, P. Valvin, T. Guillet, B. Gil, F. Ivaldi, S. Kret, and N. Grandjean, "Thermal annealing of molecular beam epitaxy-grown InGaN/GaN single quantum well," Semicond. Sci. Technol. **27**, 105023 (2012).
80. C.-C. Chuo, C.-M. Lee, T.-E. Nee, and J.-I. Chyi, "Effects of thermal annealing on the luminescence and structural properties of high indium-content InGaN/GaN quantum wells," Appl. Phys. Lett. **76**, 3902–3904 (2000).
81. S. Y. Woo, M. Bugnet, H. P. Nguyen, Z. Mi, and G. A. Botton, "Atomic ordering in InGaN alloys within nanowire heterostructures," Nano Lett. **15**, 6413–6418 (2015).
82. Y.-H. Ra, R. T. Rashid, X. Liu, S. M. Sadaf, K. Mashooq, and Z. Mi, "An electrically pumped surface-emitting semiconductor green laser," Sci. Adv. **6**, eaav7523 (2020).
83. L. Nicolai, Ž. Gačević, E. Calleja, and A. Trampert, "Electron tomography of pencil-shaped GaN/(In,Ga)N core-shell nanowires," Nano. Res. Lett. **14**, 232 (2019).
84. Z. A. Gačević, M. Holmes, E. Chernysheva, M. Müller, A. Torres-Pardo, P. Veit, F. Bertram, J. R. Christen, J. M. A. González Calbet, and Y. Arakawa, "Emission of linearly polarized single photons from quantum dots contained in nonpolar, semipolar, and polar sections of pencil-like InGaN/GaN nanowires," ACS Photon. **4**, 657–664 (2017).
85. G. Stringfellow, "The importance of lattice mismatch in the growth of Ga_xIn_{1-x} P epitaxial crystals," J. Appl. Phys. **43**, 3455–3460 (1972).
86. Y. Kawaguchi, M. Shimizu, M. Yamaguchi, K. Hiramatsu, N. Sawaki, W. Taki, H. Tsuda, N. Kuwano, K. Oki, and T. Zheleva, "The formation of crystalline defects and crystal growth mechanism in $In_xGa_{1-x}N$/GaN heterostructure grown by metalorganic vapor phase epitaxy," J. Cryst. Growth **189**, 24–28 (1998).
87. D. Queren, M. Schillgalies, A. Avramescu, G. Brüderl, A. Laubsch, S. Lutgen, and U. Strauß, "Quality and thermal stability of thin InGaN films," J. Cryst. Growth **311**, 2933–2936 (2009).
88. C.-C. Chuo, M. N. Chang, F.-M. Pan, C.-M. Lee, and J.-I. Chyi, "Effect of composition inhomogeneity on the photoluminescence of InGaN/GaN multiple quantum wells upon thermal annealing," Appl. Phys. Lett. **80**, 1138–1140 (2002).
89. C.-C. Chuo, C.-M. Lee, and J.-I. Chyi, "Interdiffusion of In and Ga in InGaN/GaN multiple quantum wells," Appl. Phys. Lett. **78**, 314–316 (2001).
90. H. Wang, Z. Ji, S. Qu, G. Wang, Y. Jiang, B. Liu, X. Xu, and H. Mino, "Influence of excitation power and temperature on photoluminescence in InGaN/GaN multiple quantum wells," Opt. Express **20**, 3932–3940 (2012).
91. S. Marcinkevičius, K. Gelžinytė, Y. Zhao, S. Nakamura, S. DenBaars, and J. Speck, "Carrier redistribution between different potential sites in semipolar $(20\bar{2}1)$ InGaN quantum wells studied by near-field photoluminescence," Appl. Phys. Lett. **105**, 111108 (2014).
92. S. Chichibu, T. Azuhata, T. Sota, and S. Nakamura, "Spontaneous emission of localized excitons in InGaN single and multiquantum well structures," Appl. Phys. Lett. **69**, 4188–4190 (1996).
93. Y. Robin, M. Pristovsek, H. Amano, F. Oehler, R. Oliver, and C. Humphreys, "What is red? On the chromaticity of orange-red InGaN/GaN based LEDs," J. Appl. Phys. **124**, 183102 (2018).
94. Y. H. Ra, R. T. Rashid, X. Liu, J. Lee, and Z. Mi, "Scalable nanowire photonic crystals: Molding the light emission of InGaN," Adv. Funct. Mater. **27**, 1702364 (2017).
95. X. Liu, Y. Wu, Y. Malhotra, Y. Sun, and Z. Mi, "Micrometer scale InGaN green light emitting diodes with ultra-stable operation," Appl. Phys. Lett. **117**, 011104 (2020).
96. C. Zhao, T. K. Ng, A. Prabaswara, M. Conroy, S. Jahangir, T. Frost, J. O'Connell, J. D. Holmes, P. J. Parbrook, and P. Bhattacharya, "An enhanced surface passivation effect in InGaN/GaN disk-in-nanowire light emitting diodes for mitigating Shockley–Read–Hall recombination," Nanoscale **7**, 16658–16665 (2015).
97. W. Liu, D. Zhao, D. Jiang, P. Chen, Z. Liu, J. Zhu, X. Li, F. Liang, J. Liu, and L. Zhang, "Shockley–Read–Hall recombination and efficiency droop in InGaN/GaN multiple-quantum-well green light-emitting diodes," J. Phys. D **49**, 145104 (2016).
98. X. Liu, Y. Sun, Y. Malhotra, A. Pandey, Y. Wu, K. Sun, and Z. Mi, "High efficiency InGaN nanowire tunnel junction green micro-LEDs," Appl. Phys. Lett. **119**, 141110 (2021).
99. X. Liu, K. Mashooq, T. Szkopek, and Z. Mi, "Improving the efficiency of transverse magnetic polarized emission from AlGaN based LEDs by using nanowire photonic crystal," IEEE Photon. J. **10**, 4501211 (2018).

100. M. G. Kibria, R. Qiao, W. Yang, I. Boukahil, X. Kong, F. A. Chowdhury, M. L. Trudeau, W. Ji, H. Guo, and F. Himpsel, "Atomic-scale origin of long-term stability and high performance of p-GaN nanowire arrays for photocatalytic overall pure water splitting," Adv. Mater. **28**, 8388–8397 (2016).
101. A. David and M. J. Grundmann, "Droop in InGaN light-emitting diodes: a differential carrier lifetime analysis," Appl. Phys. Lett. **96**, 103504 (2010).
102. A. Laubsch, M. Sabathil, W. Bergbauer, M. Strassburg, H. Lugauer, M. Peter, S. Lutgen, N. Linder, K. Streubel, and J. Hader, "On the origin of IQE-'droop' in InGaN LEDs," Phys. Status Solidi C **6**, S913–S916 (2009).
103. G. Verzellesi, D. Saguatti, M. Meneghini, F. Bertazzi, M. Goano, G. Meneghesso, and E. Zanoni, "Efficiency droop in InGaN/GaN blue light-emitting diodes: physical mechanisms and remedies," J. Appl. Phys. **114**, 071101 (2013).
104. H. Zhao, G. Liu, R. A. Arif, and N. Tansu, "Current injection efficiency induced efficiency-droop in InGaN quantum well light-emitting diodes," Solid-State Electron. **54**, 1119–1124 (2010).
105. J. Iveland, L. Martinelli, J. Peretti, J. S. Speck, and C. Weisbuch, "Direct measurement of Auger electrons emitted from a semiconductor light-emitting diode under electrical injection: identification of the dominant mechanism for efficiency droop," Phys. Rev. Lett. **110**, 177406 (2013).
106. X. Liu, Y. Sun, Y. Malhotra, A. Pandey, P. Wang, Y. Wu, K. Sun, and Z. Mi, "N-polar InGaN nanowires: breaking the efficiency bottleneck of nano and micro LEDs," Photon. Res. **10**, 587–593 (2021).
107. J. Wang, E. C. Young, W. Y. Ho, B. Bonef, T. Margalith, and J. S. Speck, "III-nitride blue light-emitting diodes utilizing hybrid tunnel junction with low excess voltage," Semicond. Sci. Technol. **35**, 125026 (2020).